Nickel-based superalloy architectures with surface mechanical attrition treatment

Cheng, Lizi; Zhang, Xiaofeng; Xu, Jiacheng; Olugbade, Temitope Olumide; Li, Gan; Dong, Dongdong

DOI:
10.1016/j.nanoms.2023.11.008

Publication date:
2024

Nano Materials Science xxx (xxxx) xxx

Contents lists available at ScienceDirect

Nano Materials Science

journal homepage: www.keaipublishing.com/cn/journals/nano-materials-science/

Nickel-based superalloy architectures with surface mechanical attrition treatment: Compressive properties and collapse behaviour

Lizi Cheng [a,b,c], Xiaofeng Zhang [b,d], Jiacheng Xu [b], Temitope Olumide Olugbade [b,e], Gan Li [b], Dongdong Dong [d], Fucong Lyu [b], Haojie Kong [b], Mengke Huo [b], Jian Lu [a,b,f,*]

[a] CityU-Shenzhen Futian Research Institute, Shenzhen, China
[b] Department of Mechanical Engineering, City University of Hong Kong, Hong Kong, China
[c] Department of Engineering, University of Cambridge, Cambridge, UK
[d] National Engineering Laboratory for Modern Materials Surface Engineering Technology & The Key Lab of Guangdong for Modern Surface Engineering Technology, Institute of New Materials, Guangdong Academy of Science, 510650, Guangzhou, China
[e] Mechanical and Electronic Engineering Department, School of Science and Engineering, University of Dundee, Dundee, UK
[f] Centre for Advanced Structural Materials, City University of Hong Kong Shenzhen Research Institute, Greater Bay Joint Division, Shenyang National Laboratory for Materials Science, Shenzhen, China

ARTICLE INFO

Keywords:
Architected materials
Selective laser melting
Surface mechanical attrition treatment
Structural analysis
Ductile alloy

ABSTRACT

Surface modifications can introduce natural gradients or structural hierarchy into human-made microlattices, making them simultaneously strong and tough. Herein, we describe our investigations of the mechanical properties and the underlying mechanisms of additively manufactured nickel–chromium superalloy (IN625) microlattices after surface mechanical attrition treatment (SMAT). Our results demonstrated that SMAT increased the yielding strength of these microlattices by more than 64.71% and also triggered a transition in their mechanical behaviour. Two primary failure modes were distinguished: weak global deformation, and layer-by-layer collapse, with the latter enhanced by SMAT. The significantly improved mechanical performance was attributable to the ultrafine and hard graded-nanograin layer induced by SMAT, which effectively leveraged the material and structural effects. These results were further validated by finite element analysis. This work provides insight into collapse behaviour and should facilitate the design of ultralight yet buckling-resistant cellular materials.

1. Introduction

Selective laser melting (SLM) technique has facilitated the efficient manufacturing of Ni-based superalloys with greater geometrical complexity and enhanced mechanical properties compared to traditional way [1]. The mechanical behaviors, deformation behaviors, and collapse modes of metallic microlattices have been extensively and systematically investigated [2,3]. Different architectures deform by a combination of strut bending, twisting, and stretching when subjected to macroscopic loads. In general, the deformation modes of strut-based or skeletal/sheet-triply periodic minimal surface-based cellular metals can be classified as either stretching-dominated (e.g., octet trusses [4]) or bending-dominated (e.g., Kelvin foams [5]). Bending-dominated structures feature a deformation plateau after yielding, and have higher toughness and consequently lower strength than stretching-dominated structures [6].

However, even stretching-dominated architectures exhibit an unstable deformation mode when their weight decreases. For example, an octet truss with a relative density of 5% exhibited a twisting mode, and only if the weight was increased by at least six times was the formation of a stable global deformation mode triggered [7]. Additionally, inherent defects, such as residual stress and poor surface finishing during the SLM fabrication process [8], can significantly weaken the mechanical properties of SLM components and make ultralight bending-dominated microlattices even weaker.

Hence, the collapse behavior of SLM components can be rather complicated. Previous studies have identified the following four categories of collapse behavior, with each corresponding to progressively weaker mechanical performance: (i) the formation of 45° shear bands immediately after the peak stress, (ii) layer-by-layer failure of the horizontal layers of the cells, (iii) global deformation, and (iv) bi-stability behavior in ultralow density materials. Many studies have used

* Corresponding author. CityU-Shenzhen Futian Research Institute, Shenzhen, China.
E-mail address: jianlu@cityu.edu.hk (J. Lu).

https://doi.org/10.1016/j.nanoms.2023.11.008
Received 29 June 2023; Accepted 7 October 2023
Available online xxxx

architectural design to trigger mode transitions that improve mechanical performance, such as by mimicking the grain-boundary orientations of crystalline materials to strengthen their lattices [9] or introducing helical beams to trigger a brittle-to-ductile transition [10]. Despite the collapse mechanism being primarily associated with its geometry [11], research has not yet considered subtractive changes; thus, the study in this paper takes the characteristics of solid materials into account, rather than focusing on the architectural design or thickening of the structure for better load capacity.

As-built additive manufacturing components usually exhibit rough surfaces, which is a problem because materials usually tend to fail on the surface. To mitigate or eliminate such detrimental effects, it has been shown that the mechanical property of SLM components with nearly full density can be significantly enhanced through post-processing, such as by heat treatment [12], hot isostatic pressing (HIP) treatment [13], as well as impact-based surface treatments [14] like shot peening, abrasive blasting, ball impact treatment, laser shock peening, and ultrasonic surface mechanical attrition treatment (SMAT) [15,16].

Lightweight metallic lattices, with a ratio of strut diameter to unit cell size (t/d) < 0.1, are fragile and delicate, although they remain desirable given their outstanding mechanical properties [17]. However, normal post-processing may distort the final geometry and induce cracks in lightweight metallic lattices [18]. The velocity of the flying ball in SMAT is controllable and lower than the conventional shot peening velocity of about 100 m/s, and this makes SMAT useful for processing such as intricate geometries [19]. HIP is another effective way to reduce internal pores in SLM components, but struggles to close surface cracks [20]. DebRoy et al. also reported that the HIP process can cause recrystallisation and coarsen microstructures, which leads to strength decrease [21]. Same as HIP, Maskery et al. found that heat treatment increased the ductility of lattices composed of the aluminum alloy AlSi10Mg, despite sacrificing 12% tensile strength of the base materials and 25% of the metallic Al–Si10–Mg lattice [22]. For the Inconel625 (IN625) superalloy, pores escaped in the dendrite arms of the fusion zone during rapid cooling in heat treatment, directly leading to micropores and precipitation of small Laves phases around them [23]. In addition, all of these post-processing operations are time-consuming and expensive [24].

SMAT is an effective way to introduce ultra-fine grains or nanograins into the surface of materials, as it can accumulate small plastic deformations with random strain directions, resulting in the increased strength of crystalline materials [25–27]. Previous studies have shown that SMAT is an effective post-processing technique for improving the microstructure and mechanical properties of additively manufactured titanium components, as it enhances their fatigue strength by 100% [15]. However, compared to conventional flat plates, fewer study show SMAT technology applied to elaborate components.

As Ni alloys are particularly ductile [28], such alloys would be more amenable to SMAT than heat treatment or HIP. Furthermore, the open-cell configuration such as truncated octahedral cells, would facilitate the passage of the bombardment balls into their complex structures and thus ensure uniform SMAT.

Thus, this paper describes a simple one-step SMAT process was developed to enhance the mechanical properties of Ni-based superalloy architectures. While existing studies have explored deformation behaviors and collapse modes of metallic microlattices, a significant gap remains in comprehending the intricate collapse behavior of complex architectures without creating new structures or incorporating new materials. By investigating the introduction of an ultrafine grain layer, this research significantly enhances the mechanical performance of microlattices, further leveraging material and structural effects, and introduces a novel approach for improving materials like nickel-based high-temperature alloys. Since optimal SMAT processes vary with architectures and strut size, the most common ultralight open-cell porous materials—Kelvin foams was investigated from experimental and theoretical perspectives.

2. Materials and methods

2.1. Sample fabrication (Materials and SLM parameters)

The macro/microstructures were 3D-printed via SLM under nitrogen atmosphere on an M290 3D printer (EOS, Germany), using powdered IN625 alloy (ultimate tensile strength of as-built SLM IN625 alloy is 760 MPa; Carpenter Technology Corporation, USA), and then post-processed via SMAT. Fig. 1 shows a schematic illustrations of SLM (Fig. 1(a)) and SMAT (Fig. 1(b)). In SLM, a layer of atomized metal powder (with a grain size of approximately 35.8 μm) is initially spread across a steel bedplate. A regulated laser path and exposure time melt powder selectively. The process is repeated with a new layer of powder and laser processing until it gradually builds up complex geometry.

In SMAT, ultrasonically stimulated high-speed flying balls strike a target material. The material, size, and speed of the bombardment balls used in the SMAT process directly determine the bombardment energy impacting the specimen [29]. Insufficient treatment leads to only minor enhancements of material hardness and strength, minimizing the benefits of the surface attrition. By contrast, over-treatment (i.e., when the grain size cannot be further refined) causes specimens to buckle or bend, which may lead to the formation of surface microcracks. This is a particular problem for specimens with elaborate details, and thus grain refinement and mechanical enhancement are criteria used for determining the optimal working parameters for SMAT. Based on our experiments and previous research [30], we selected a low vibration frequency of 20 Hz and 304 stainless steel balls with a diameter of 0.8 mm, which is smaller than the pore diameter of the open-cell lattices. Each lattice face was

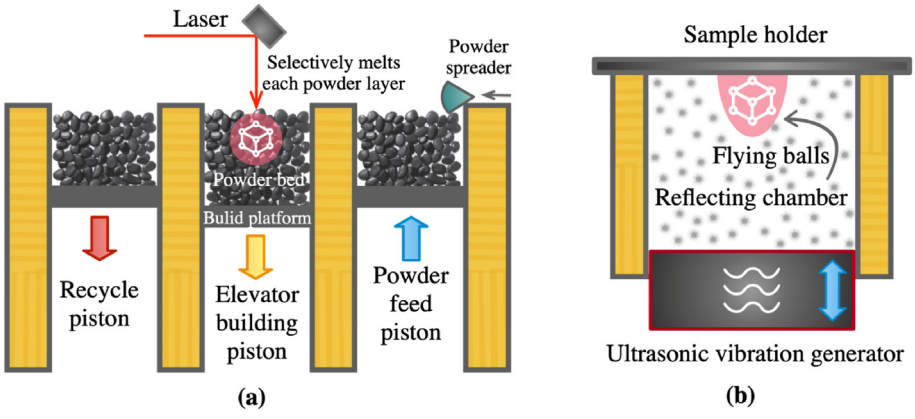

Fig. 1. Schematic illustrations of as-built and surface mechanical attrition treated (SMATed) microlattices. (a) Fabrication by selective laser melting (SLM) of an IN625 microlattice. (b) Diagram of the SMAT setup, with 304 stainless balls of diameters of 0.8 mm, which are smaller than the pore diameters of the lattices.

Table 1
Chemical composition of IN625 powder used in this study, wt%. (provided by the manufacturer).

Sample (wt%)	Ni	Cr	Fe	Mo	Nb	C	Mn	Si	Al	Ti	Co
Power	Bal.	21.70	2.8	8.8	3.9	0.03	0.2	0.3	0.01	0.03	0.01

Table 2
Parameters used in 3D printing of IN625 lattices.

Parameter	Value
Laser power	255 W
Laser beam spot	80 μm
Powder layer thickness	40 μm
Beam scan velocity	0.96 m/s
Hatching distance	110 μm

subjected to SMAT for 20 min at room temperature. We also tried SMAT for 10, 15, and 20 min on each lattice face. However, only the 20-min case showed obvious grain refinement under SEM, which was the primary focus of our work in assessing the SMAT effect on the lattice. Additionally, it trigger the transition in deformation behavior. Therefore, we selected a 20-min treatment duration for this experiment, as it demonstrated the desired effects on the lattice.

The constituent materials of the as-built lattice were determined by energy-dispersive X-ray spectroscopy (EDS) and the powder used in this study are detailed in Table 1, in accordance with industry standards for high-efficiency turbine machinery production [28]. Lattice building parameters used are listed in Table 2. A rotated scanning path (at 67°) between the layers was adopted to reduce the thermal stress buildup during the formation process. The mass loss after SMAT was negligible (<0.1%).

2.2. Mechanical characterization

In situ uniaxial compression tests were conducted to observe lattice deformation behavior at room temperature, using an MTS RT/30 Electro-Mechanical Material Testing System and a high-speed video camera (Canon). The mechanical properties of the lattice were characterized in displacement-control mode at a constant strain rate of 10^{-3}/s. All compression tests were conducted on at least three parallel specimens. In data presentations, the error bars represent the scatters. Engineering stresses were obtained using the nominal cross-sectional areas, and strains were calculated from the change in height of the structures [31, 32]. The yield strength was determined by the offset method at 2% strain. For porous materials, the critical parameters were porosity ($P = 1 - \overline{\rho}$) and relative density $\overline{\rho}$. Here, $\overline{\rho}$ is defined as the ratio of the measured lattice density (ρ) to the solid bulk material (ρ_0). The specific compressive strength ($\overline{\sigma} = \sigma_y/\rho$) was calculated from the yield strength of the lattice (σ_y) and measured lattice density.

2.3. Microstructural characterization

We further examined the strengthening mechanism of SMATed lattice via hardness tests, electron backscatter diffraction (EBSD) analysis, and transmission electron microscopy (TEM). The hardness (H) of the as-built and SMATed sample surfaces was determined using a nanoindenter (Hysitron, USA). We polished a lattice normal to the building direction and exposed its cross-section to obtain the relationship between hardness and depth along its surface, and nanoindentation was performed using a Berkovich diamond tip at a load of 4000 μN, with the indenter tip area function calibrated on fused silica. EBSD patterns were used characterize the crystal size and texture of a cross-section at a voltage of 15 kV at room temperature. Before EBSD analysis, samples were electropolished in a solution of 1:4 mixture of nitric acid:ethanol for 30 s. EBSD maps of 200 μm × 200 μm were obtained, with a scanning step size of 0.1 μm. Part of the cross-sectional strut of each SMATed specimen was extracted by focused ion beam (FIB) for high-resolution transmission electron microscopy (HRTEM) analysis.

2.4. Finite elements calculations

The different deformation behaviors were verified through a numerical simulation conducted using ANSYS software. A static analysis approach was employed to model the compression process of the material. The simulation involved applying displacement at the top of the model while keeping the bottom fixed to simulate the compression conditions. Additionally, a Poisson's ratio of 0.3 was assigned to the material to account for its transverse strain response.

Constitutive models for the Ni alloys solid material were derived based on experimental tensile tests [33]. Regarding the effect of SMAT treatment, it is worth noting that in this study, the SMAT treatment primarily targeted the ultrafine strut in lattice structure. Therefore, the same SMAT parameters do not have significant effects on standard dog-bone specimen (Standard ASTM E1820). Although conducting direct tensile experiments poses certain is challenge and considering the gradient material properties after SMAT treatment is complex, existing research on SMAT-treated nickel alloys consistently supports the notion that SMAT primarily enhanced the yield strength while the Young's modulus remains unchanged. Therefore, in order to simplify the problem, we leveraged relevant data from the literature specifically related to SMAT-treated nickel alloys [33]. These data served as a foundation for reasonably estimating the material behavior after SMAT treatment, thus enabling prediction of the material's mechanical response in the numerical simulation.

3. Results

3.1. Microstructural characterization

The ultralight as-built and SMATed lattice specimens are shown in Fig. 2(a). Through repeated physical impacts, the high-speed flying balls produced multidirectional plastic deformations on the surface of specimens. Consequently, the surface of SMATed lattices was glossy and smooth, unlike the rough surfaces of their as-built counterparts (see Fig. 2(b)). To verify the uniformity of the SMAT processing, we examined the innermost beam of a lattice. As shown in Fig. 2(c and d), the innermost beam had black spots similar to those in the outermost beam, indicating that SMAT successfully introduced uniform nanograins within the entire 3D architecture.

3.2. Mechanical characterization

Manufacturing defects are a major cause of degraded mechanical properties, but it is difficult to determine a general trend among the effects of manufacturing defects, as each defect needs to be analyzed on a case-by-case basis. Two distinct deformation signatures were found: (i) uniform deformation spread throughout the entire lattice, and (ii) ductile-like layer-by-layer collapse. The as-built Kelvin foams exhibited the typical stress-strain response (Fig. 3(a and b)) of a soft or light material [34]. This response features an elastic loading zone, followed by a plateau regime with almost constant stress, which corresponds to a uniform deformation, as indicated in Fig. 3(c). In contrast, rather than exhibiting a flat plateau or brittle high-frequency oscillations, the stress–strain curve of the SMATed lattices resembled a ductile-like stable

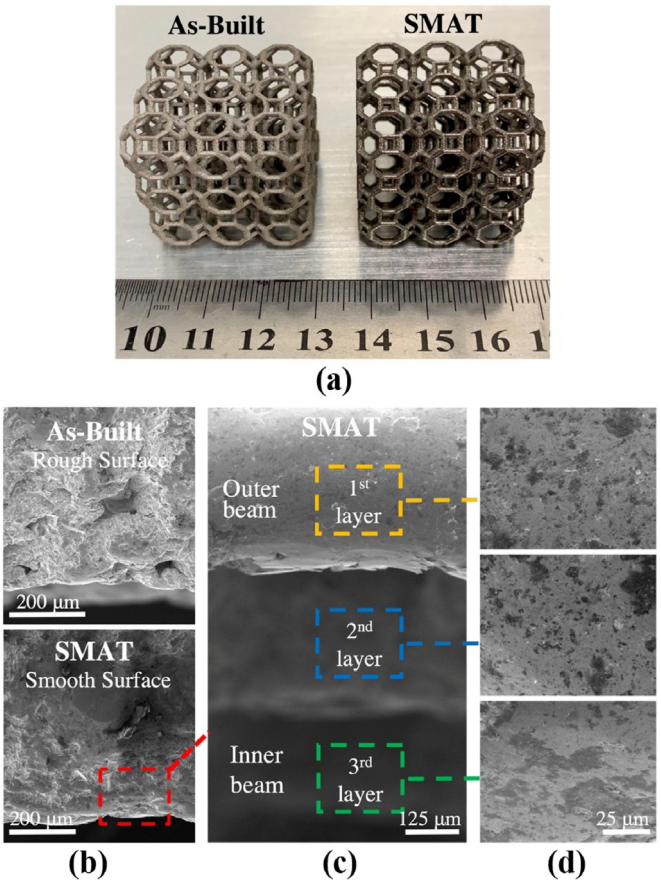

Fig. 2. Microstructural characterization of as-built and SMATed open-cell microlattices. (a) Overview of a whole specimen. (b) Microstructural characterization showing surface roughness. (c) The multi-layer struts in the lattice, which can be seen after tilting the sample stage by 15° in SEM. (d) The magnified SEM image of the inner, middle, and outer struts.

wave after yielding. In situ observations of this large plastic deformation revealed that each peak corresponded to the collapse of a layer, starting with the boundary layers and ending with the middle layer. Consequently, their specific strength increased significantly by 64.71% (Fig. 3(b)). In contrast, their Young's moduli were nearly unaffected by SMAT, which is consistent with previous findings on the effects of SMAT [35,36].

4. Discussion and mechanism

The deformation pattern was distinguished by initial global bending and progressive (layer-by-layer) collapse. The failure criterion during lattice compression was an active competition between buckling and the strength of the base material. The discussion below considers both solid material and FEA validated configuration.

4.1. Solid materials

Measurements of the nanoindentations on the IN625 specimens revealed that the as-built and SMAT-treated lattice base materials differed in their hardness. It is clearly shown that SMAT favoured an increase of hardness from 63% to 26% as a function of depth in Fig. 4. The maximum nanohardness of SMATed SLM IN625 alloys was increased to near 7 GPa from 4 GPa, which is consistent with previous studies. The Berkovich nano-indentation hardness of the C-2000 alloy ranged from 3 GPa to 7 GPa after surface-severe-plastic-deformation [37]. The as-built SLM Inconel 718 alloy surface possesses a relatively high nano-hardness above 4 GPa [38]. The nanohardness variety with the depth from the peened surface of Ni3Al from 4 GPa to 12 GPa [39]. Although the result may influenced by the size of the sample and degree of SMAT, the variety of nanohardness with depth showed the enhanced hardness of the peened surface than matrix. This increase in hardness can be attributed to the grain refinement associated with a more compact morphology and a layer of nanograins. Such fine microstructures are desirable as they improve the fatigue performance and strength of a specimen.

The EBSD patterns in Fig. 5 show that the grain sizes of the as-built IN625 were approximately 50 μm. In a face-centered cubic (fcc) IN625 specimen fabricated through SLM, the grain structure is primarily characterized by columnar grains. This columnar grain formation is a result of thermal gradients and epitaxial growth [40], with the solidification growth direction aligning along <001>, in accordance with the building direction [41]. Some of these grains span several hundred micrometers, and the presence of such large columnar grains makes it more likely for subgrains to form, similar to the plastic deformation induced by shot peening in SLM built IN625 alloys [42]. In our SMAT sample, there was a gradient distribution of grain size, which increases from the matrix (left) to the surface (right). Severe distortion and limited EBSD resolution made it difficult to characterize the nanocrystalline features. Therefore, part of the cross-sectional strut of the SMATed specimen was extracted via FIB for TEM analysis.

Fig. 6 (a, b) shows a typical high-magnification TEM image of the graded grain-size distribution from the surface to the core. The inner core was far from the surface and was therefore regarded as a non-SMAT-affected zone. The image shows there were disordered atoms in the SMAT-affected zone, suggesting that the topmost surface had undergone severe plastic deformation. The selected area electron diffraction (SAED) pattern was nearly a complete ring, indicating that highly refined nanoscale grains were distributed with random crystallographic orientations. The HRTEM image also showed the ordered atoms in the core, and the corresponding well-defined SAED further confirmed the presence of coarse grains and the formation of the fcc phase.

4.2. Finite element calculations

For lattices with slender beams, the dominant failure mechanism is material-dependent [43]. The two deformation modes are consistent with the numerical prediction as showed in Fig. 7. The top layer of the as-built specimens is less deformable compared to that of the SMATed samples, instead, it features with a weaker global deformation. Since the pioneering work of Lu et al. [44–46], who first found and analyzed how SMAT-induced nanostructured surface layers can make metallic bulk structures stronger but brittle, few researchers have investigated SMAT effects on lattice materials. In representative stress-strain curves of ductile alloys after SMAT treatment [35,36] as shown in Fig. 8(a), the brittle or a mixture of brittle and ductile failure mechanisms of an SMATed sample leads to limited elongation. The yield strength σy was significantly improved despite Young's modulus (slope k_1) being almost unchanged. When applied to a lattice, SMAT triggers the transition from initial global deformation to progressive collapse, because the trend of the plastic stage (refer to k_2) matters. If the k_2 approaches 0 (typically brittle), lattice can achieve layer-by-layer deformation. On the contrary, if the k_2 is not much from that of the elastic region, such as work hardening in ductile metals, the response reflects on the lattice is global deformation.

This transformation in deformation behavior is fundamentally tied to the mechanical properties of solid materials. To answer the question of when the deformation mode transitions from one state to another in the kelvin foam lattice, we conducted an in-depth mechanics analysis on the material parameters of the solid, namely the yield strength (σ_y) and

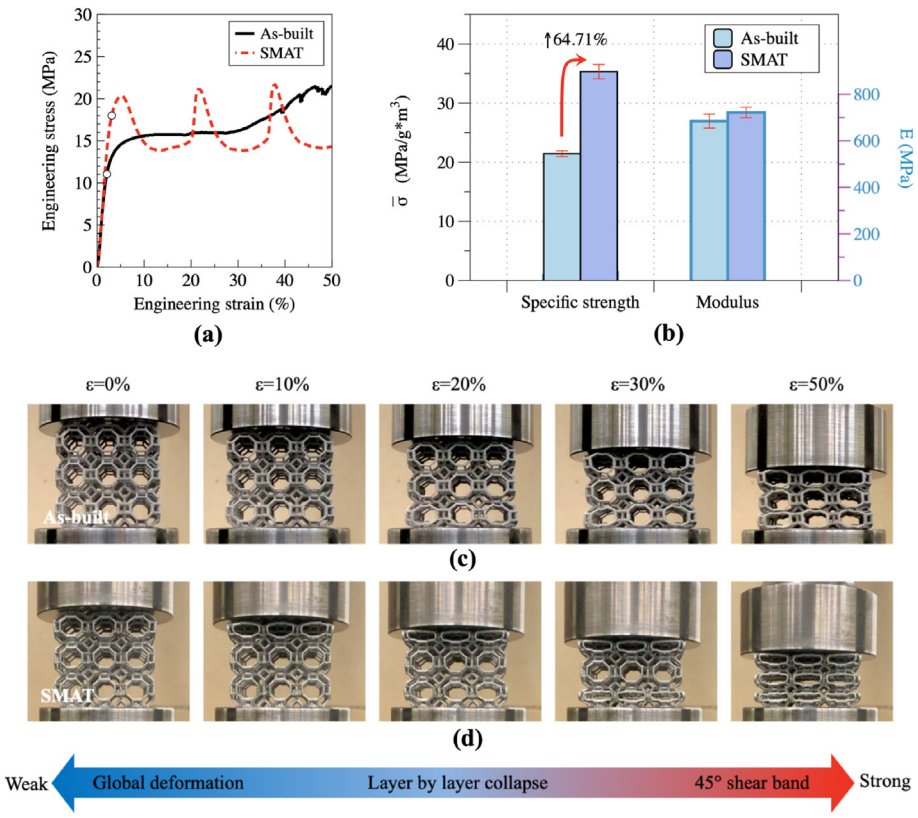

Fig. 3. Experimental compressive response of as-built and SMATed lattices: (a) engineering stress–strain curve; (b) Comparison of specific strength and Young's modulus; data are shown as means ± SDs; (c, d) snapshots captured at compression = 50 %.

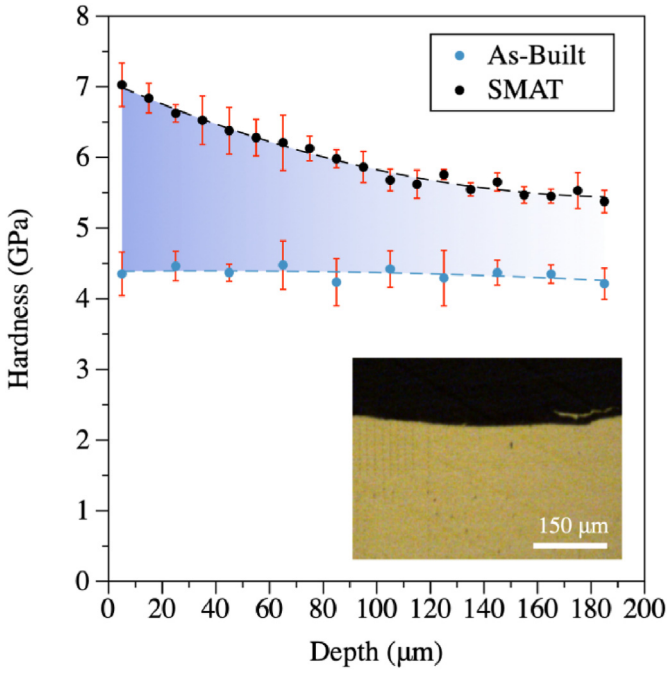

Fig. 4. Mechanical property comparisons of solid materials, which explained the distinguished deformation pattern of the lattice. Berkovich nanoindentation hardness distribution along the cross-section of the surface of the beam obtained from SMATed lattices compared to as-built 3D architecture. Insert image was obtained by optical microscope, indicated the tested area starts from the edge of the sample.

plastic stage slope (k_2 at a plastic strain of 0.2). With a fixed Young's modulus of 50 GPa as our reference point, we systematically investigated the relationship between these material parameters and the observed deformation modes. A mapping of the material parameter shifts that trigger this transition is presented in Fig. 8(b), shedding light on the intricate interplay between the properties of base material and the deformation of the lattice.

Lattice materials may fail when the local stress in a given cell reaches the tensile/compressive strength of the base material or when local buckling occurs. When the two aforementioned failure modes compete in lightweight lattice materials, buckling dominates [47]. Our microlattices had a relative density of only 5.91 ± 0.02%, and thus their slenderness ratios rendered them susceptible to a global plastic collapse. During laser melting, geometric defects and cracks are generated on the surfaces, particularly at rough minor nodes. Because of the structures' slenderness, the metal particles are loosely bonded and the region where these initial defects accumulate is the first to undergo distortion during the loading process. Thus, after SMAT, the cracks on the rough surface closed and the metal particles on each strut became more densely compressed than before SMAT.

4.3. Gibson-Ashby crushing strength formula

A pioneering study showed that a column fails by either global bending or progressive buckling, depending on the slenderness ratio [48]. The stiffness and strength of stretching-dominated structures scales linearly as a function of the relative density (i.e., $\overline{\rho} = \rho/\rho_0$), whereas bending-dominated structures scale quadratically. Kelvin foam, whose stiffness and strength are governed by the bending stiffness of the cell edges [49], has an experimental yield stress that scales with measured lattice density (ρ) following the analytical predictions of Gibson and

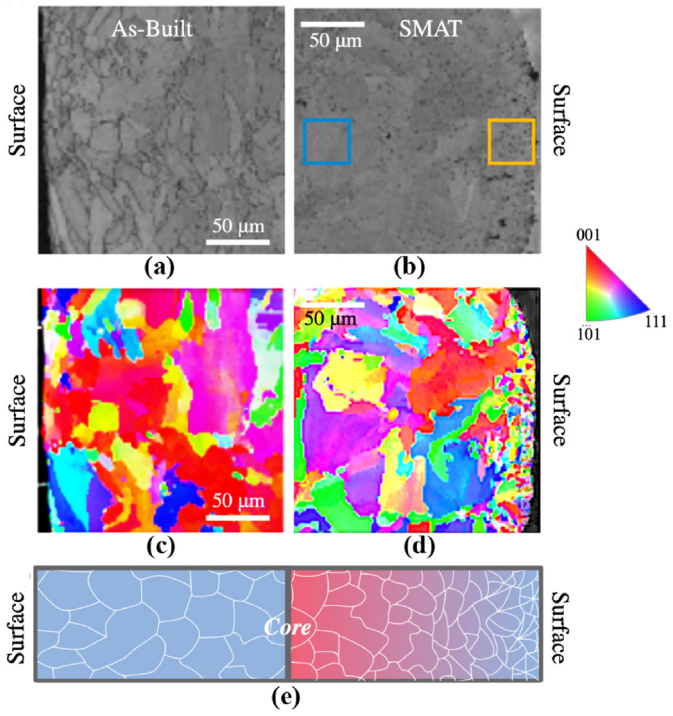

Fig. 5. Microstructures comparisons of solid materials, which explained the distinguished deformation pattern of the lattice. Cross-sectional SEM images of (a) as-built and (b) SMAT IN625, and corresponding cross-sectional electron backscatter diffraction (EBSD) images in (c) and (d), respectively. (e) Schematic drawings of the grains on as-built and SMATed surfaces.

Ashby, which were based on a point-wise stress-based failure criterion [50–52], as indicated in Eq. (1). Therefore, the relationship between relative density and compressive strength can be expressed by a power law, shown in Eq. (2) as follows:

$$\sigma_y \approx a\,\sigma_0\,\rho^m, \text{ with } 1.5 \le m \le 2.0 \quad \text{(Eq. 1)}$$

$$\sigma_y \approx b\,\sigma_0\,\bar{\rho}^m, \text{ with } 1.5 \le m \le 2.0 \quad \text{(Eq. 2)}$$

where σ_0 and E_0 are the yield stress and Young's modulus for the bulk materials, respectively, and a and b are constants related to geometry. For bending-dominated architectures, the scaling exponent, m, is generally in the range of 1.5–2.0. For example, m = 1.5 for an ideal tetrakaidecahedron lattice. SMAT improves the solid strength associated with the yield stress at the node, and the buckling stress, thereby endowing a beam with excellent resistance to plastic buckling.

In practical applications and for mass production, it is crucial to improve the strength of sizeable lightweight lattices. However, the various shortcomings of SLM and configuration processes make the fabrication of ultralight lattice materials difficult. According to the Gibson–Ashby crushing strength formula, the minimum weight design for a prescribed bending compressive strength is as shown in Fig. 9(a). In contrast with the unfavorable as-built lattice, the SMATed lattice shows a pronounced weight reduction (28.68–40.00%) under the same load capacity.

To check the geometric fidelity in terms of relative density, we scaled down the 3D model and printed lattice (3*3*3 units) with cell sizes of 3.33, 5 and 10 mm. Theoretical relative density ($\bar{\rho}_0$) was based on CAD, while SLM manufacturing increased the relative density ($\bar{\rho}$). We calculated the percentage error in relative density as $(\bar{\rho}\text{-}\bar{\rho}_0)/\bar{\rho}_0$ to quantify the deviation. Consistent with previous studies [53], the actual measured

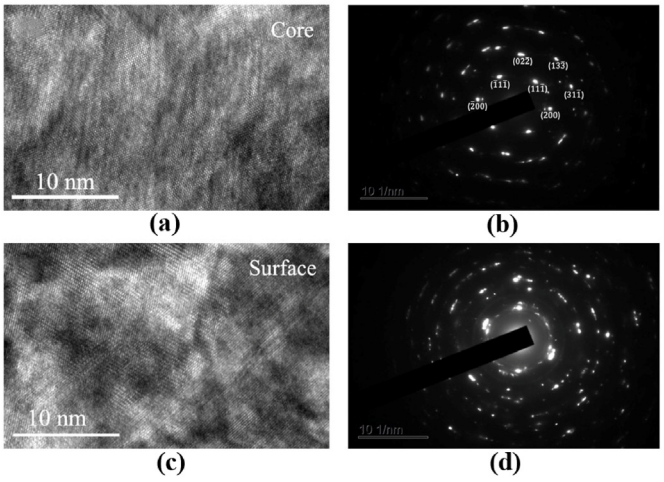

Fig. 6. High-resolution transmission electron microscopy images from the (a) inner area to the (c) surface of the SMAT sample, with their corresponding selected diffraction patterns shown in the (b) and (d).

relative density of the as-built lattice is larger than theoretical value, and the standard error of the relative density decreases with the size of the unit cell (Fig. 9(b)). Possible explanations for this include: (i) processing parameters were selected that resulted in the as-built samples having the smallest possible feature sizes; (ii) the cross-sectional diameter of a strut increased with the strut inclination angle during laser etching [54]; (iii) the SLM process tended to remove adhered powder particles neighboring the melt pool during fabrication (i.e, those particles not subjected to other post-processing (e.g., sand-blasting, ultrasonic cleaning, chemical etching)) [53].

The error for our as-built specimens is within 5% of the design values. Because most structures require precise control of the relative density and fine internal structure, large cellular lattices are more reliable in terms of geometric fidelity than other lattices. However, lattice materials, particularly in low-density structures, are subject to a size effect, such that larger lattices have lower strength than smaller lattices. This is because the buckling strength scales with the unit cell parameter d according to d^{-2} [52]. So the larger the unit size, the weaker the buckling strength and the greater the tendency for buckling.

Research has long been focused on improving bulk materials or the design of innovative structures [52]. However, the relationship between structures and materials is synergistic; i.e., a certain structure can amplify the strengthen of a solid material. Strengthening architectures to trigger the deformation transition has been accomplished before, with collapse mechanisms known to be primarily governed by their topology and strut thickness [7,55,56]. Most previous studies have focused on changing architectural design, such as by developing precipitation hardening of crystal-inspired designs [57,58], grain-boundary hardening for brittle-to-ductile transitions [9], and graded cellular structures for uniform-to-successive deformation [55,56]. Other studies have focused on post-processing to enhance the base materials, which originate from techniques using bulk materials [59]. Nevertheless, not all post-processing techniques applied to bulk materials have positive effects when applied to lattice materials, as indicated in Fig. 9(c). It can be seen that SMAT provide a new way and has certain advantages among all technologies, despite the fact that accurate comparisons are difficult due to limited literature and various materials.

5. Conclusions

SMAT was identified as an advanced post-processing treatment for

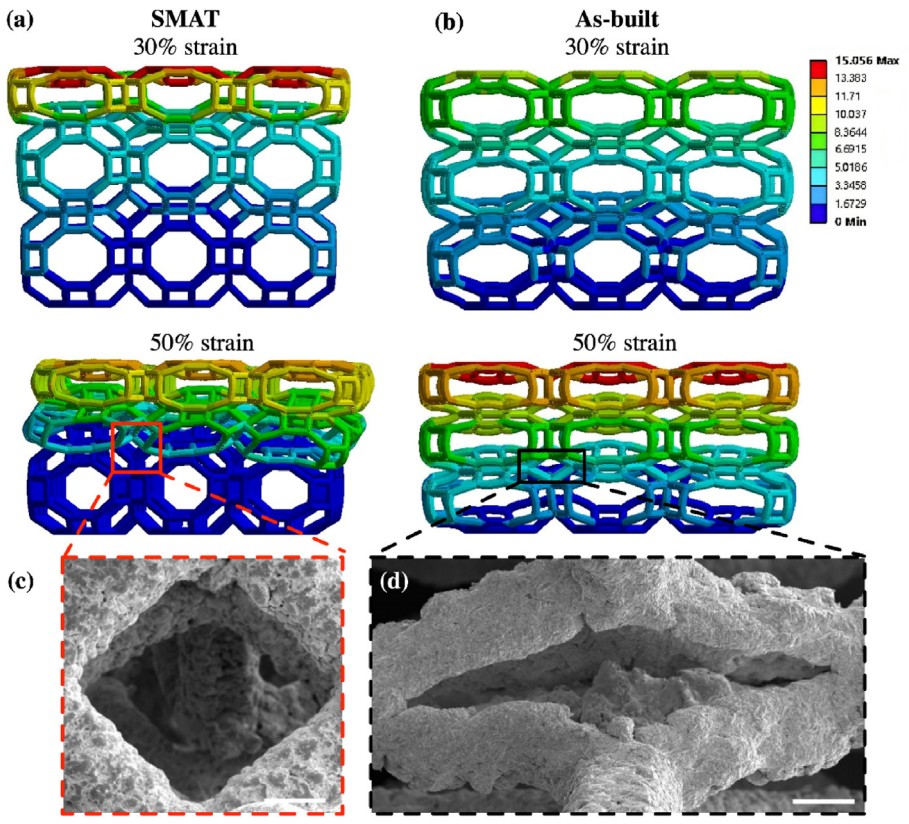

Fig. 7. Finite element analysis of a microlattice under large deformation. (a) SMATed and (b) As-built lattice with the nominal strain first at 30% (above) then at 50% (below). After 50% strain, the corresponding SEM images (c) and (d) characterize the difference of deformed area, as well as the roughness and distortion of the as-built lattice. Scale bars, 1 μm.

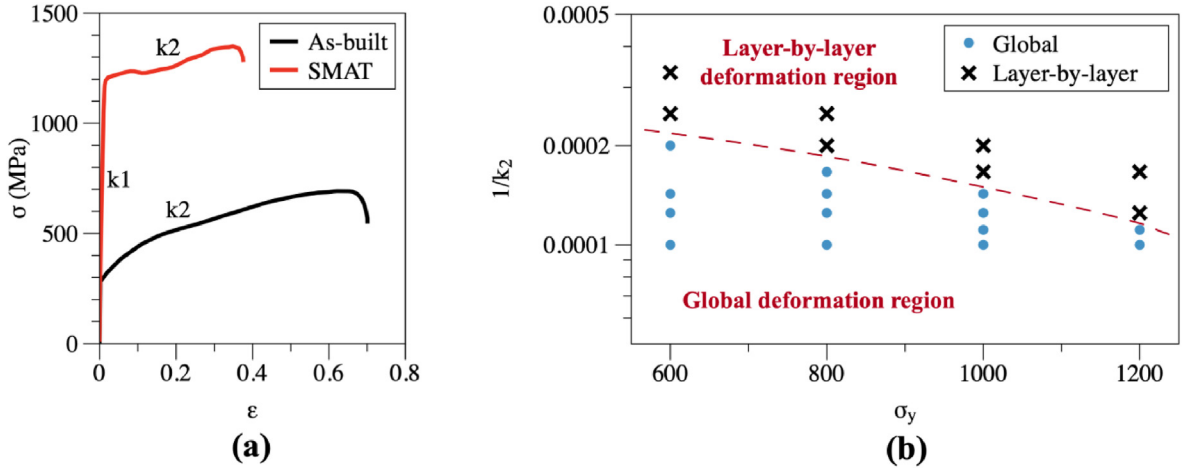

Fig. 8. Mechanics analysis on material properties and deformation mode in KF lattice. (a) Representative stress-strain curves of ductile alloys after SMAT treatment. (b) Material parameter-driven deformation transition.

complex 3D architectures and a suitable treatment for ultralight IN625 lattices to minimize their susceptibility to early global buckling. In ultralight microlattices, SMAT triggered the transition of the deformation mode from global deformation to a layer-by-layer collapse. Nanoindentation measurements, EBSD, and TEM observations confirmed that SMAT introduced an ultrahard nanocrystalline layer onto the surface of a lattice, thereby enhancing the mechanical properties of the base materials, which in turn affected the deformation mode of the architecture. Specifically, SMAT increased the yield strength by 64.71%. Moreover, a transition of the density-dependent deformation mode was achieved, leading to a 28.68–40.00% weight loss under the same load capacity. This work offers a promising route to applying SMAT to architected materials and may open new avenues for strengthening ultralight complex metal parts with good structural fidelity.

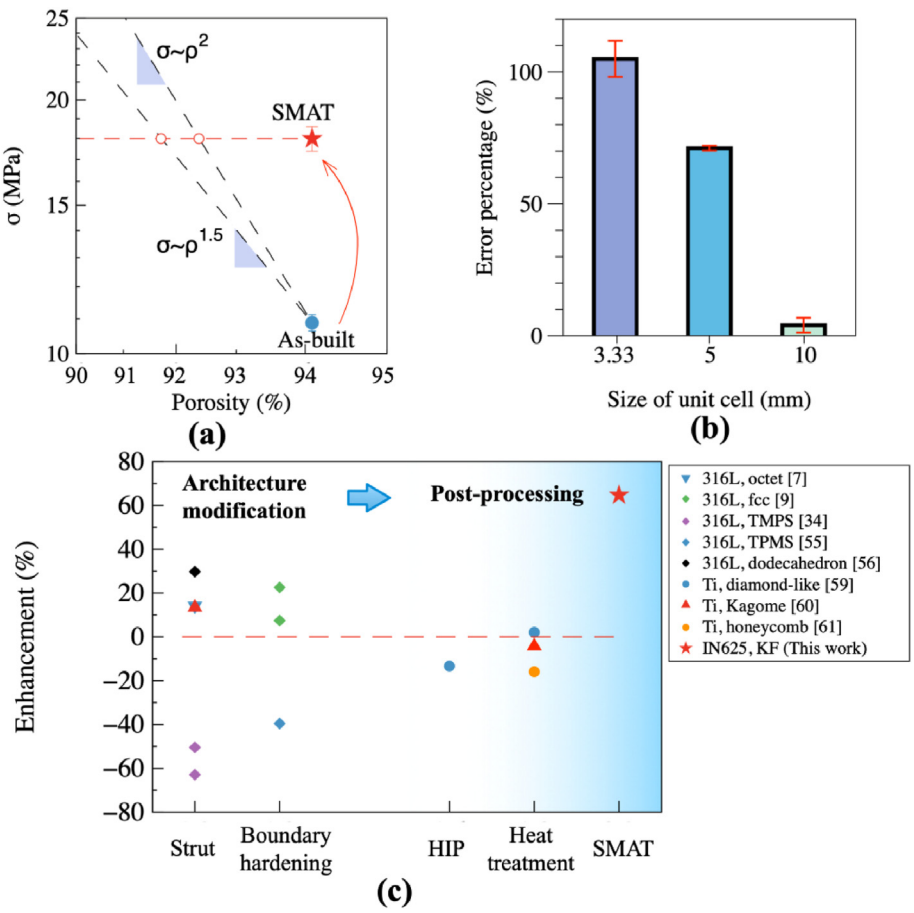

Fig. 9. Mechanical enhancement based on Gibson–Ashby theory. (a) Strength scales with porosity, indicating that SMAT can reduce a lattice's appreciable weight. (b) The influence of the unit cell size on percentage error in relative density $(\bar{\rho}\text{-}\bar{\rho}_0)/\bar{\rho}_0$, demonstrating the more delicate geometric fidelity of larger unit cells, whose mechanical property can especially be enhanced by SMAT. (c) Compressive strength enhancement after architecture modification and post-processing lattice materials with transition of deformation mode [7,9,34,55,56,59–61].

Declaration of competing interest

Jian Lu is an Editor-in-Chief for [Nano Materials Science] and was not involved in the editorial review or the decision to publish this article. All authors declare that there are no competing interests.

Acknowledgements

J. Lu gratefully acknowledges the financial support provided by Shenzhen-Hong Kong Science and Technology Innovation Cooperation Zone Shenzhen Park Project: HZQB-KCZYB-2020030, the Hong Kong General Research Fund (GRF) Scheme (Ref: CityU 11216219), the Research Grants Council of Hong Kong (Project No: AoE/M-402/20), Shenzhen Science and Technology Program: JCYJ20220818101204010, and the Hong Kong Innovation and Technology Commission via the Hong Kong Branch of National Precious Metals Material Engineering Research Center.

References

[1] C. Guo, G. Li, S. Li, X. Hu, H. Lu, X. Li, Z. Xu, Y. Chen, Q. Li, J. Lu, Additive manufacturing of Ni-based superalloys: residual stress, mechanisms of crack formation and strategies for crack inhibition, Nano Materials Science (2022).
[2] N. Jin, F. Wang, Y. Wang, B. Zhang, H. Cheng, H. Zhang, Effect of structural parameters on mechanical properties of Pyramidal Kagome lattice material under impact loading, Int. J. Impact Eng. 132 (2019) 103313.
[3] M. Benedetti, A. du Plessis, R.O. Ritchie, M. Dallago, S.M.J. Razavi, F. Berto, Architected cellular materials: a review on their mechanical properties towards fatigue-tolerant design and fabrication, Mater. Sci. Eng. R Rep. 144 (2021).
[4] V.S. Deshpande, N.A. Fleck, M.F. Ashby, Effective properties of the octet-truss lattice material, J. Mech. Phys. Solid. 49 (8) (2001) 1747–1769.
[5] L. Gong, S. Kyriakides, N. Triantafyllidis, On the stability of Kelvin cell foams under compressive loads, J. Mech. Phys. Solid. 53 (4) (2005) 771–794.
[6] X. Zheng, H. Lee, T.H. Weisgraber, M. Shusteff, J. DeOtte, E.B. Duoss, J.D. Kuntz, M.M. Biener, Q. Ge, J.A. Jackson, S.O. Kucheyev, N.X. Fang, C.M. Spadaccini, Ultralight, ultrastiff mechanical metamaterials, Science 344 (6190) (2014) 1373–1377.
[7] T. Tancogne-Dejean, A.B. Spierings, D. Mohr, Additively-manufactured metallic micro-lattice materials for high specific energy absorption under static and dynamic loading, Acta Mater. 116 (2016) 14–28.
[8] R.R. Srivastava, M.-s. Kim, J.-c. Lee, M.K. Jha, B.-S. Kim, Resource recycling of superalloys and hydrometallurgical challenges, J. Mater. Sci. 49 (14) (2014) 4671–4686.
[9] M.S. Pham, C. Liu, I. Todd, J. Lertthanasarn, Damage-tolerant architected materials inspired by crystal microstructure, Nature 565 (7739) (2019) 305–311.
[10] L. Cheng, T. Tang, H. Yang, F. Hao, G. Wu, F. Lyu, Y. Bu, Y. Zhao, Y. Zhao, G. Liu, X. Cheng, J. Lu, The twisting of dome-like metamaterial from brittle to ductile, Adv. Sci. (2021) 2002701.
[11] O. Al-Ketan, R. Rowshan, R.K. Abu Al-Rub, Topology-mechanical property relationship of 3D printed strut, skeletal, and sheet based periodic metallic cellular materials, Addit. Manuf. 19 (2018) 167–183.
[12] C. Chang, X. Yan, R. Bolot, J. Gardan, S. Gao, M. Liu, H. Liao, M. Chemkhi, S. Deng, Influence of post-heat treatments on the mechanical properties of CX stainless steel fabricated by selective laser melting, J. Mater. Sci. 55 (19) (2020) 8303–8316.
[13] D.K. Pattanayak, A. Fukuda, T. Matsushita, M. Takemoto, S. Fujibayashi, K. Sasaki, N. Nishida, T. Nakamura, T. Kokubo, Bioactive Ti metal analogous to human cancellous bone: fabrication by selective laser melting and chemical treatments, Acta Biomater. 7 (3) (2011) 1398–1406.
[14] M. Kumagai, K. Kimura, N. Shimada, M. Ishiwata, Inhomogeneous strain and recrystallisation of a shot-peened Inconel 625 alloy after annealing, Mater. Sci. Technol. 35 (15) (2019) 1856–1863.
[15] X. Yan, S. Yin, C. Chen, R. Jenkins, R. Lupoi, R. Bolot, W. Ma, M. Kuang, H. Liao, J. Lu, M. Liu, Fatigue strength improvement of selective laser melted Ti6Al4V using ultrasonic surface mechanical attrition, Materials Research Letters 7 (8) (2019) 327–333.
[16] S. Ghosh, N. Bibhanshu, S. Suwas, K. Chatterjee, Surface mechanical attrition treatment of additively manufactured 316L stainless steel yields gradient nanostructure with superior strength and ductility, Mater. Sci. Eng., A 820 (2021) 141540.

[17] T.A. Schaedler, A.J. Jacobsen, A. Torrents, A.E. Sorensen, J. Lian, J.R. Greer, L. Valdevit, W.B. Carter, Ultralight metallic microlattices, Science 334 (6058) (2011) 962–965.
[18] N. Sanaei, A. Fatemi, Defects in additive manufactured metals and their effect on fatigue performance: a state-of-the-art review, Prog. Mater. Sci. (2020).
[19] B.A. Raj, J. Jappes, M.A. Khan, V. Dillibabu, N.R. Jesudoss Hynes, Studies on mechanical attrition and surface analysis on heat-treated nickel alloy developed through additive manufacturing, Adv. Mater. Sci. Eng. (2022) 2022.
[20] X. Gong, T. Anderson, K. Chou, Review on powder-based electron beam additive manufacturing technology, in: International Symposium on Flexible Automation, American Society of Mechanical Engineers, 2012, pp. 507–515.
[21] T. DebRoy, H. Wei, J. Zuback, T. Mukherjee, J. Elmer, J. Milewski, A.M. Beese, A.d. Wilson-Heid, A. De, W. Zhang, Additive manufacturing of metallic components–process, structure and properties, Prog. Mater. Sci. 92 (2018) 112–224.
[22] I. Maskery, N.T. Aboulkhair, A.O. Aremu, C.J. Tuck, I.A. Ashcroft, Compressive failure modes and energy absorption in additively manufactured double gyroid lattices, Addit. Manuf. 16 (2017) 24–29.
[23] Y. Zhang, X. Hu, Y. Jiang, Study on the microstructure and fatigue behavior of a laser-welded Ni-based alloy manufactured by selective laser melting method, J. Mater. Eng. Perform. 29 (5) (2020) 2957–2968.
[24] K. Mumtaz, N. Hopkinson, Selective Laser Melting of Inconel 625 Using Pulse Shaping, Rapid Prototyping Journal, 2010.
[25] X. Chen, J. Lu, L. Lu, K. Lu, Tensile properties of a nanocrystalline 316L austenitic stainless steel, Scripta Mater. 52 (10) (2005) 1039–1044.
[26] H.L. Chan, H.H. Ruan, A.Y. Chen, J. Lu, Optimization of the strain rate to achieve exceptional mechanical properties of 304 stainless steel using high speed ultrasonic surface mechanical attrition treatment, Acta Mater. 58 (15) (2010) 5086–5096.
[27] A. Chen, H. Ruan, J. Wang, H. Chan, Q. Wang, Q. Li, J. Lu, The influence of strain rate on the microstructure transition of 304 stainless steel, Acta Mater. 59 (9) (2011) 3697–3709.
[28] R.C. Reed, The Superalloys: Fundamentals and Applications, Cambridge university press, 2008.
[29] W. Tsai, J. Huang, Y.J. Gao, Y. Chung, G.-R. Huang, Relationship between microstructure and properties for ultrasonic surface mechanical attrition treatment, Scripta Mater. 103 (2015) 45–48.
[30] T. Wegener, T. Wu, F. Sun, C. Wang, J. Lu, T. Niendorf, Influence of surface mechanical attrition treatment (SMAT) on microstructure, tensile and low-cycle fatigue behavior of additively manufactured stainless steel 316L, Metals 12 (9) (2022) 1425.
[31] P. Köhnen, C. Haase, J. Bültmann, S. Ziegler, J.H. Schleifenbaum, W. Bleck, Mechanical properties and deformation behavior of additively manufactured lattice structures of stainless steel, Mater. Des. 145 (2018) 205–217.
[32] X. Feng, J.U. Surjadi, R. Fan, X. Li, W. Zhou, S. Zhao, Y. Lu, Microalloyed medium-entropy alloy (MEA) composite nanolattices with ultrahigh toughness and cyclability, Mater. Today 42 (2021) 10–16.
[33] S. Cao, Mechanical Properties and Fretting Fatigue of SMAT-Treated Stainless Steels and Nickel-Based Alloys, City University of Hong Kong, 2016.
[34] C. Bonatti, D. Mohr, Smooth-shell metamaterials of cubic symmetry: anisotropic elasticity, yield strength and specific energy absorption, Acta Mater. 164 (2019) 301–321.
[35] S.C. Cao, J. Liu, L. Zhu, L. Li, M. Dao, J. Lu, R.O. Ritchie, Nature-inspired hierarchical steels, Sci. Rep. 8 (1) (2018) 5088.
[36] X. Cao, D. Zhang, B. Liao, S. Fang, L. Liu, R. Gao, Y. Li, Numerical analysis of the mechanical behavior and energy absorption of a novel P-lattice, Thin-Walled Struct. 157 (2020).
[37] L.L. Shaw, J. Villegas, J.-Y. Huang, S. Chen, Strengthening via deformation twinning in a nickel alloy, Mater. Sci. Eng., A 480 (1–2) (2008) 75–83.
[38] Z. Baicheng, L. Xiaohua, B. Jiaming, G. Junfeng, W. Pan, S. Chen-nan, N. Muiling, Q. Guojun, W. Jun, Study of selective laser melting (SLM) Inconel 718 part surface improvement by electrochemical polishing, Mater. Des. 116 (2017) 531–537.
[39] J. Ren, A. Shan, J. Zhang, H. Song, J. Liu, Surface nanocrystallization of Ni3Al by surface mechanical attrition treatment, Mater. Lett. 60 (17–18) (2006) 2076–2079.
[40] K. Amato, S. Gaytan, L.E. Murr, E. Martinez, P. Shindo, J. Hernandez, S. Collins, F. Medina, Microstructures and mechanical behavior of Inconel 718 fabricated by selective laser melting, Acta Mater. 60 (5) (2012) 2229–2239.
[41] C. Pleass, S. Jothi, Influence of powder characteristics and additive manufacturing process parameters on the microstructure and mechanical behaviour of Inconel 625 fabricated by Selective Laser Melting, Addit. Manuf. 24 (2018) 419–431.
[42] M. Balbaa, A. Ghasemi, E. Fereiduni, K. Al-Rubaie, M. Elbestawi, Improvement of fatigue performance of laser powder bed fusion fabricated IN625 and IN718 superalloys via shot peening, J. Mater. Process. Technol. 304 (2022) 117571.
[43] I. Quintana-Alonso, S. Mai, N. Fleck, D. Oakes, M. Twigg, The fracture toughness of a cordierite square lattice, Acta Mater. 58 (1) (2010) 201–207.
[44] W. Tong, N. Tao, Z. Wang, J. Lu, K. Lu, Nitriding iron at lower temperatures, Science 299 (5607) (2003) 686–688.
[45] K. Lu, J. Lu, Nanostructured surface layer on metallic materials induced by surface mechanical attrition treatment, Mater. Sci. Eng., A 375 (2004) 38–45.
[46] T.O. Olugbade, J. Lu, Literature review on the mechanical properties of materials after surface mechanical attrition treatment (SMAT), Nano Materials Science 2 (1) (2020) 3–31.
[47] N.A. Fleck, Micro-architectured Solids: from Blast Resistant Structures to Morphing Wings, Mechanics Down Under, Springer, 2013, pp. 57–65.
[48] W. Abramowicz, N. Jones, Transition from initial global bending to progressive buckling of tubes loaded statically and dynamically, Int. J. Impact Eng. 19 (5–6) (1997) 415–437.
[49] S. Pingle, N. Fleck, V. Deshpande, H. Wadley, Collapse mechanism maps for a hollow pyramidal lattice, Proc. R. Soc. A 467 (2128) (2011) 985–1011.
[50] M.F. Ashby, L.J. Gibson, Cellular Solids: Structure and Properties, Press Syndicate of the University of Cambridge, Cambridge, UK, 1997, pp. 175–231.
[51] M.F. Ashby, T. Evans, N.A. Fleck, J. Hutchinson, H. Wadley, L. Gibson, Metal Foams: a Design Guide, Elsevier, 2000.
[52] N.A. Fleck, V.S. Deshpande, M.F. Ashby, Micro-architectured materials: past, present and future, Proc. R. Soc. A 466 (2121) (2010) 2495–2516.
[53] M. Leary, M. Mazur, H. Williams, E. Yang, A. Alghamdi, B. Lozanovski, X. Zhang, D. Shidid, L. Farahbod-Sternahl, G. Witt, I. Kelbassa, P. Choong, M. Qian, M. Brandt, Inconel 625 lattice structures manufactured by selective laser melting (SLM): mechanical properties, deformation and failure modes, Mater. Des. 157 (2018) 179–199.
[54] M. Mazur, M. Leary, S. Sun, M. Vcelka, D. Shidid, M. Brandt, Deformation and failure behaviour of Ti-6Al-4V lattice structures manufactured by selective laser melting (SLM), Int. J. Adv. Des. Manuf. Technol. 84 (5) (2016) 1391–1411.
[55] L. Yang, R. Mertens, M. Ferrucci, C. Yan, Y. Shi, S. Yang, Continuous graded Gyroid cellular structures fabricated by selective laser melting: design, manufacturing and mechanical properties, Mater. Des. 162 (2019) 394–404.
[56] X. Cao, D. Xiao, Y. Li, W. Wen, T. Zhao, Z. Chen, Y. Jiang, D. Fang, Dynamic compressive behavior of a modified additively manufactured rhombic dodecahedron 316L stainless steel lattice structure, Thin-Walled Struct. 148 (2020) 106586.
[57] J. Lertthanasarn, C. Liu, M. Pham, Synergistic effects of crystalline microstructure, architected mesostructure, and processing defects on the mechanical behaviour of Ti6Al4V meta-crystals, Mater. Sci. Eng., A 818 (2021) 141436.
[58] C. Liu, J. Lertthanasarn, M.-S. Pham, The origin of the boundary strengthening in polycrystal-inspired architected materials, Nat. Commun. 12 (1) (2021) 1–10.
[59] R. Wauthle, B. Vrancken, B. Beynaerts, K. Jorissen, J. Schrooten, J.-P. Kruth, J. Van Humbeeck, Effects of build orientation and heat treatment on the microstructure and mechanical properties of selective laser melted Ti6Al4V lattice structures, Addit. Manuf. 5 (2015) 77–84.
[60] R. Gautam, S. Idapalapati, Performance of strut-reinforced Kagome truss core structure under compression fabricated by selective laser melting, Mater. Des. 164 (2019).
[61] P. Baranowski, P. Płatek, A. Antolak-Dudka, M. Sarzyński, M. Kucewicz, T. Durejko, J. Małachowski, J. Janiszewski, T. Czujko, Deformation of honeycomb cellular structures manufactured with Laser Engineered Net Shaping (LENS) technology under quasi-static loading: experimental testing and simulation, Addit. Manuf. 25 (2019) 307–316.